NACA TN 3548

NATIONAL ADVISORY COMMITTEE FOR AERONAUTICS

TECHNICAL NOTE 3548

FLIGHT INVESTIGATION AT MACH NUMBERS FROM 0.6 TO 1.7 TO DETERMINE DRAG AND BASE PRESSURES ON A BLUNT-TRAILING-EDGE AIRFOIL AND DRAG OF DIAMOND AND CIRCULAR-ARC AIRFOILS AT ZERO LIFT

By John D. Morrow and Ellis Katz

Langley Aeronautical Laboratory
Langley Field, Va.

Washington
November 1955

NATIONAL ADVISORY COMMITTEE FOR AERONAUTICS

TECHNICAL NOTE 3548

FLIGHT INVESTIGATION AT MACH NUMBERS FROM 0.6 TO 1.7 TO DETERMINE DRAG AND BASE PRESSURES ON A BLUNT-TRAILING-EDGE AIRFOIL AND DRAG OF DIAMOND AND CIRCULAR-ARC AIRFOILS AT ZERO LIFT[1]

By John D. Morrow and Ellis Katz

SUMMARY

Results of an exploratory free-flight investigation at zero lift of several rocket-powered drag-research models having rectangular 6-percent-thick wings are presented for a Mach number range of 0.6 to 1.7. Wings of aspect ratio 2.7 having diamond, circular-arc, and blunt-trailing-edge airfoil sections were tested. Pressures were measured on the base of the blunt-trailing-edge airfoil which had a rectangular section with a 40-percent-chord beveled leading edge. Although the blunt-trailing-edge airfoil had high drag throughout the Mach number range investigated because of high base suction pressures, it is believed that the data presented can be used in the design of more nearly optimum blunt-base airfoils. Of the airfoils tested, the circular-arc section had lowest drag at high-subsonic speeds, and the diamond section had lowest drag at supersonic speeds.

INTRODUCTION

A great deal of research has been directed toward the determination of practical airfoils for flight at supersonic speeds. The major effort has been concentrated on sections having relatively sharp leading and trailing edges. Consideration has been given (reference 1) to airfoil sections having blunt or flat trailing edges. This type of section, it is believed, may combine favorable aerodynamic characteristics with desirable structural qualities. These favorable characteristics are possibly lower drag for the same strength, increased lift-curve slope, and increased control effectiveness in the transonic speed range.

---

[1]Supersedes declassified NACA RM L50E19a, 1950.

The design of such wing sections depends largely on the magnitude of the pressures developed over the flat base of the trailing edge. In view of the scarcity of wing base-pressure data, particularly through the transonic speed range, a flight investigation of a rocket-powered model has been made at the Langley Pilotless Aircraft Research Station at Wallops Island, Va., to determine the pressures acting over the base of a rectangular wing. The results of that test are presented in this paper. Also included for comparative purposes are tests of rocket-powered models having identical plan forms with diamond and circular-arc airfoil sections.

The wing drag presented in this paper includes the mutual interference drag between wings, body, and stabilizing fins. Results are presented for a Mach number range from 0.6 to 1.7 corresponding to a Reynolds number range from 2.8×10^6 to 9.8×10^6 based on wing chord.

SYMBOLS

C_{D_T}	total-drag coefficient based on exposed wing area of 1.389 square feet
C_{D_W}	wing drag coefficient based on exposed wing area
M	Mach number
R	Reynolds number based on wing chord
p_b	base pressure, pounds per square foot
p_o	free-stream pressure, pounds per square foot
C_{p_b}	base pressure coefficient $\left(\frac{p_b - p_o}{\frac{1}{2}\rho V^2}\right)$
W	weight of test vehicle, powder expended, pounds
a	measured acceleration, feet per second per second

g	acceleration of gravity, 32.194 feet per second per second
θ	angle between model center line and horizontal, degrees
ρ	density of air, slugs per cubic foot
V	measured velocity, feet per second
T	temperature of air, $^{\circ}F$ absolute
S	exposed wing area, square feet

MODELS

The general arrangement of the drag-research vehicles used in this investigation is shown in figures 1 to 4. The models were wooden cylinders with pointed wooden ogival noses and were stabilized with four thin metal fins located near the base. The basic model construction has been altered only for the blunt-trailing-edge model (hereinafter referred to as the slab) by the use of a metal nose and a cut-off rocket motor to allow room for the base-pressure telemetering equipment. The 6-percent-thick rectangular wings of aspect ratio 2.7 were located as shown in figure 4. The slab model had two base-pressure slits 0.02 by 2.5 inches located in the central part of the wing base. Two models each for the diamond and circular-arc sections were flown and one model having a blunt-trailing-edge section was flown. Four wingless models were also flown in order that a wing-alone drag-coefficient curve might be obtained as the difference between drags of the winged and wingless models.

The models were propelled by 3.25-inch aircraft rocket motors which were contained within the fuselage.

TESTS

The models were flown at the Pilotless Aircraft Research Station at Wallops Island, Va. The test technique consists essentially of measuring the radial distance of the model from the launching site with respect to time, ascertaining the flight path of the model, and of making an atmospheric survey at the time of firing. These measurements are taken during the coasting period of flight before maximum altitude is

reached. The data from these three sources are used in the following equations to determine the drag coefficient C_D and Mach number M for a given model:

$$C_D = \frac{-2W(a + g \sin \theta)}{g\rho SV^2}$$

$$M = \frac{V}{49.2\sqrt{T}}$$

The atmospheric quantities ρ and T are measured with respect to altitude by radiosonde and are tied into the flight history of the model by altitude-time measurements taken from the SCR 584 radar tracking unit. The angle θ is determined from the trajectory described by the SCR 584 unit by assuming the model to be flying at zero lift. The velocity and acceleration time histories are reduced from measurements taken from the CW Doppler radar velocimeter unit. The Doppler unit furnishes a time history of the straight-line distance between the model and the launching site. The velocity corrected for flight-path curvature is obtained from the first derivative of the distance-time variation and acceleration is obtained from the derivative of the corrected velocity-time curve. The method by which these two differentiations are obtained has been analytically developed to its present state of precision, which generally results in a maximum possible velocity error of less than 0.5 foot per second and an acceleration error of less than 3 feet per second per second. At points of discontinuity or very sharp inflections in the acceleration-time-history curve, the method tends to reduce the abruptness of the true variations. This distortion is due to the averaging of the acceleration over small periods of time. The probable inaccuracy in the values of wing drag coefficient are approximately ±0.002 except at the extreme ends of the Mach number range. The Mach number is believed to be accurate to within ±0.01.

The slab model was equipped with a two-channel telemeter for recording wing base pressure in two locations. The accuracy of the base pressure coefficients is estimated to be ±0.02 at a Mach number of 0.800 and ±0.005 at a Mach number of 1.400.

The average Reynolds number of the five models with wings based on wing chord (9.582 inches) varied from 2.79×10^6 at a Mach number of 0.625 up to 9.76×10^6 at a Mach number of 1.735.

RESULTS AND DISCUSSION

A plot of Reynolds number is shown in figure 5. The base pressure coefficients of the two pressure slits on the base of the slab wing are shown in figure 6 along with the base pressure coefficient of a body of revolution (reference 2) and the limiting base pressure coefficient (vacuum). The base-pressure-coefficient curve showed a very high suction peak near a Mach number of 1.0 and showed greater suction at subsonic than at supersonic speeds. These base-pressure measurements are in agreement with data presented for the bases of wedge airfoil sections in references 3 and 4. The data of reference 2, along with unpublished data, indicated that the suction over the base of a body of revolution was much less than the base suction of the slab wing in this investigation. The base-pressure slits did not necessarily measure average suction over the entire base because they were located in the central part of the base. The total drag coefficient is presented in figure 7 plotted against Mach number for the slab model and four wingless models. The base drag coefficients were converted from base pressure coefficient by multiplying by the thickness-chord ratio and are shown in figure 8 along with the slab-wing drag coefficient which was obtained by subtracting the wingless drag curve from the slab total-drag curve; also shown are the wave-drag coefficient calculated from reference 5 and the friction-drag coefficient calculated from reference 6. Except above $M \approx 1.35$, the summation of the base drag and component drag coefficients is indicated to be greater than the total wing drag coefficients. This apparent inconsistency may be due to favorable interference effects of the wing on the tail fins which are not present for the wingless models or to the fact that negative pressures may exist on the beveled leading edge of the slab at subsonic speeds which would result in a negative drag coefficient of approximately 0.003 for the beveled portion of the wing. In addition, the base drag coefficients measured are not average values but values taken over the central part of the wing base. The blunt-trailing-edge airfoil tested was not an optimum airfoil section since it had high drag throughout the Mach number range investigated. However, it is believed that the base-pressure data presented may be used in the design of more nearly optimum blunt-base airfoils and also for evaluating the drag of blunt bases added to controls for improving their transonic effectiveness.

The total-drag coefficient is presented in figure 9 plotted against Mach number for the diamond and circular-arc configurations. Data for the wingless model are included in order that the wing drag coefficient may be found. Figure 10 shows both experimental and theoretical (calculated from reference 7) wing drag coefficient plotted against Mach number. The experimental wing drag coefficient was obtained by subtracting the wingless-body drag-coefficient curve from the various winged-configuration curves. The theoretical points agree reasonably

well with experimental results. The experimental curves show that the circular-arc section had the lowest drag below a Mach number of approximately 1.1. Above $M = 1.1$, the diamond section had the lowest drag. Theoretical calculations indicate that the shock would become attached to the nose of the diamond airfoil at a Mach number of 1.18. The slab wing of the same thickness had substantially higher drag throughout the Mach number range covered in this investigation. The higher subsonic base suction discussed previously may partly explain why the differences in drag-coefficient curve (fig. 10) of the slab compared with the circular arc and diamond are more extreme at subsonic than at supersonic speeds.

CONCLUDING REMARKS

An exploratory free-flight investigation of rocket-powered drag-research models has been conducted at zero lift for a Mach number range of 0.6 to 1.7. Although the blunt-trailing-edge airfoil had high drag because of high base suction pressures, it is believed that the data presented can be used in the design of more nearly optimum blunt-base airfoils. This suction was much greater than the suction over the base of a body of revolution with similar cross section. The data also indicated that, for the three wings of equal thickness, the circular-arc section had the lowest drag at subsonic speeds and the diamond section had the lowest drag at supersonic speeds.

Langley Aeronautical Laboratory,
National Advisory Committee for Aeronautics,
Langley Field, Va., May 17, 1950.

REFERENCES

1. Chapman, Dean R.: Reduction of Profile Drag at Supersonic Velocities by the Use of Airfoil Sections Having a Blunt Trailing Edge. NACA RM A9H11, 1949.

2. Faro, I. D. V.: Experimental Determination of Base Pressures at Supersonic Velocities. Bumblebee Rep. No. 106, The Johns Hopkins Univ., Appl. Phys. Lab., Nov. 1949.

3. Valensi, J., and Pruden, F. W.: Some Observations on Sharp-Nosed Profiles at Supersonic Speed. R. & M. No. 2482, British A.R.C., May 1947.

4. Sawyer, Richard H., and Daum, Fred L.: Measurement Through the Speed of Sound of Static Pressures on the Rear of Unswept and Sweptback Circular Cylinders and on the Rear and Sides of a Wedge by the NACA Wing-Flow Method. NACA RM L8B13, 1948.

5. Ivey, H. Reese, Stickle, George W., and Schuettler, Alberta: Charts for Determining the Characteristics of Sharp-Nose Airfoils in Two-Dimensional Flow at Supersonic Speeds. NACA TN 1143, 1947.

6. Von Kármán, Th.: Turbulence and Skin Friction. Jour. Aero. Sci., vol. 1, no. 1, Jan. 1934, pp. 1-20.

7. Bonney, E. Arthur: Aerodynamic Characteristics of Rectangular Wings at Supersonic Speeds. Jour. Aero. Sci., vol. 14, no. 2, Feb. 1947, pp. 110-116.

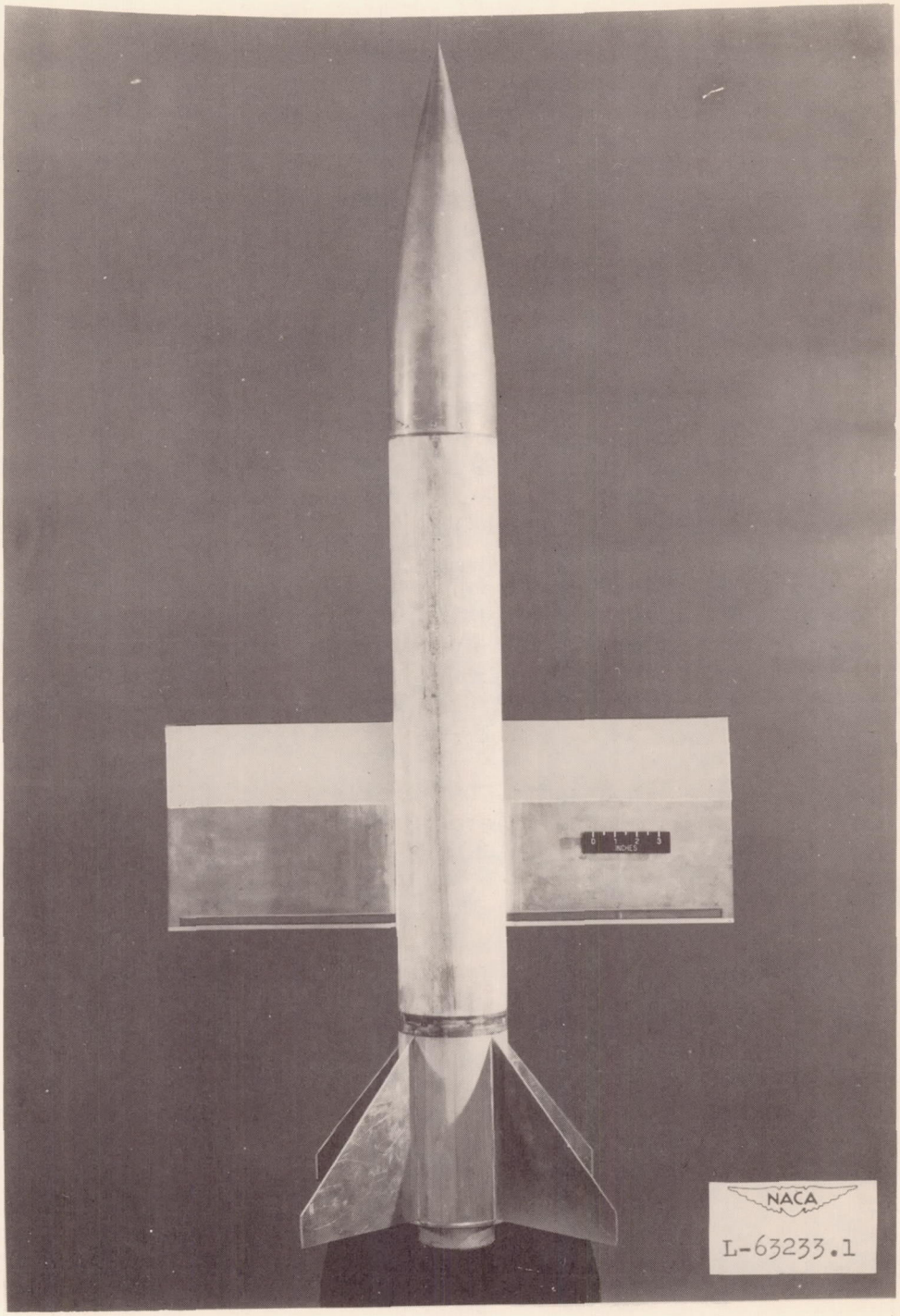

(a) Plan-form view.

Figure 1.- Photograph showing general arrangement of slab-wing vehicle and location of pressure slits.

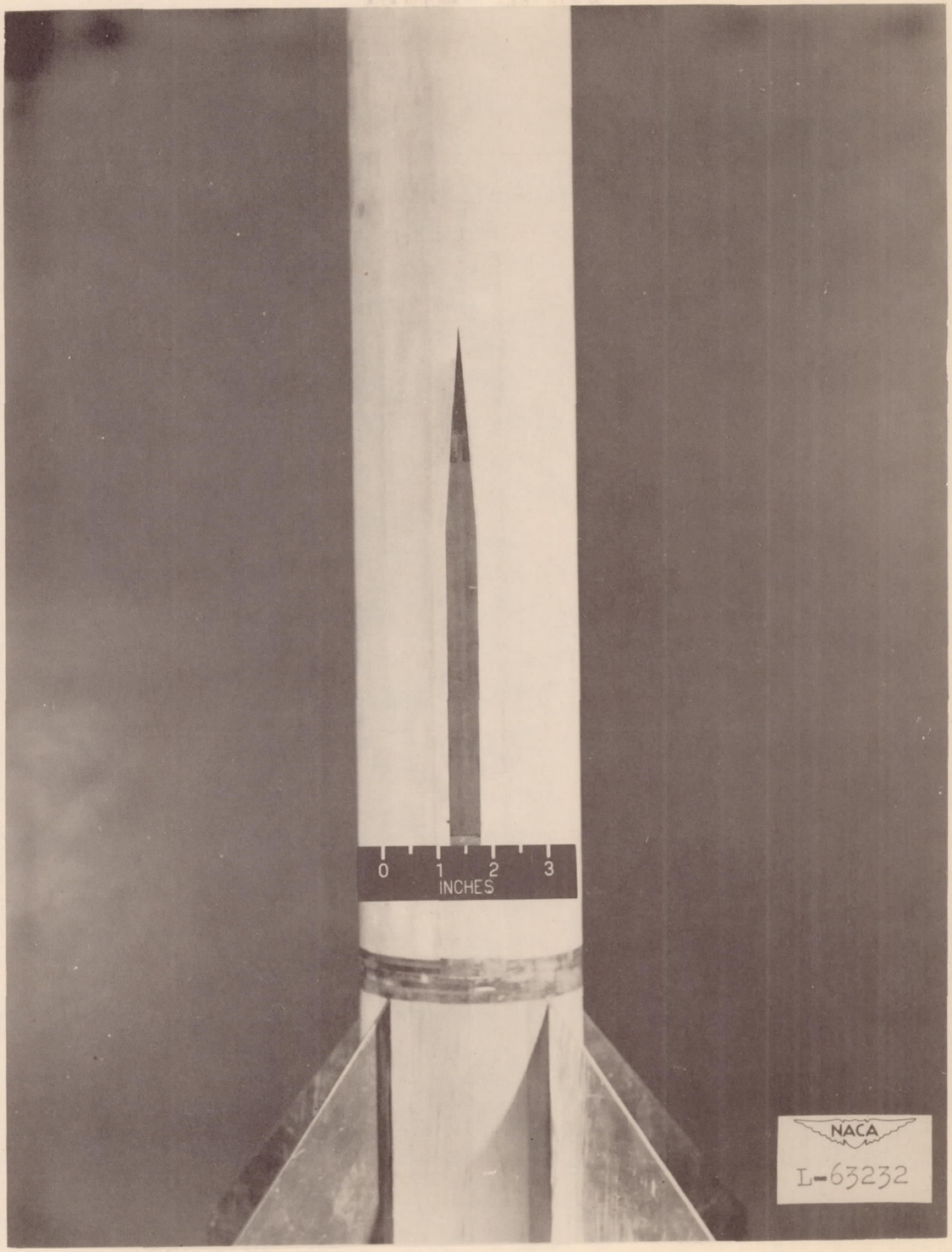

(b) Wing section.

Figure 1.- Continued.

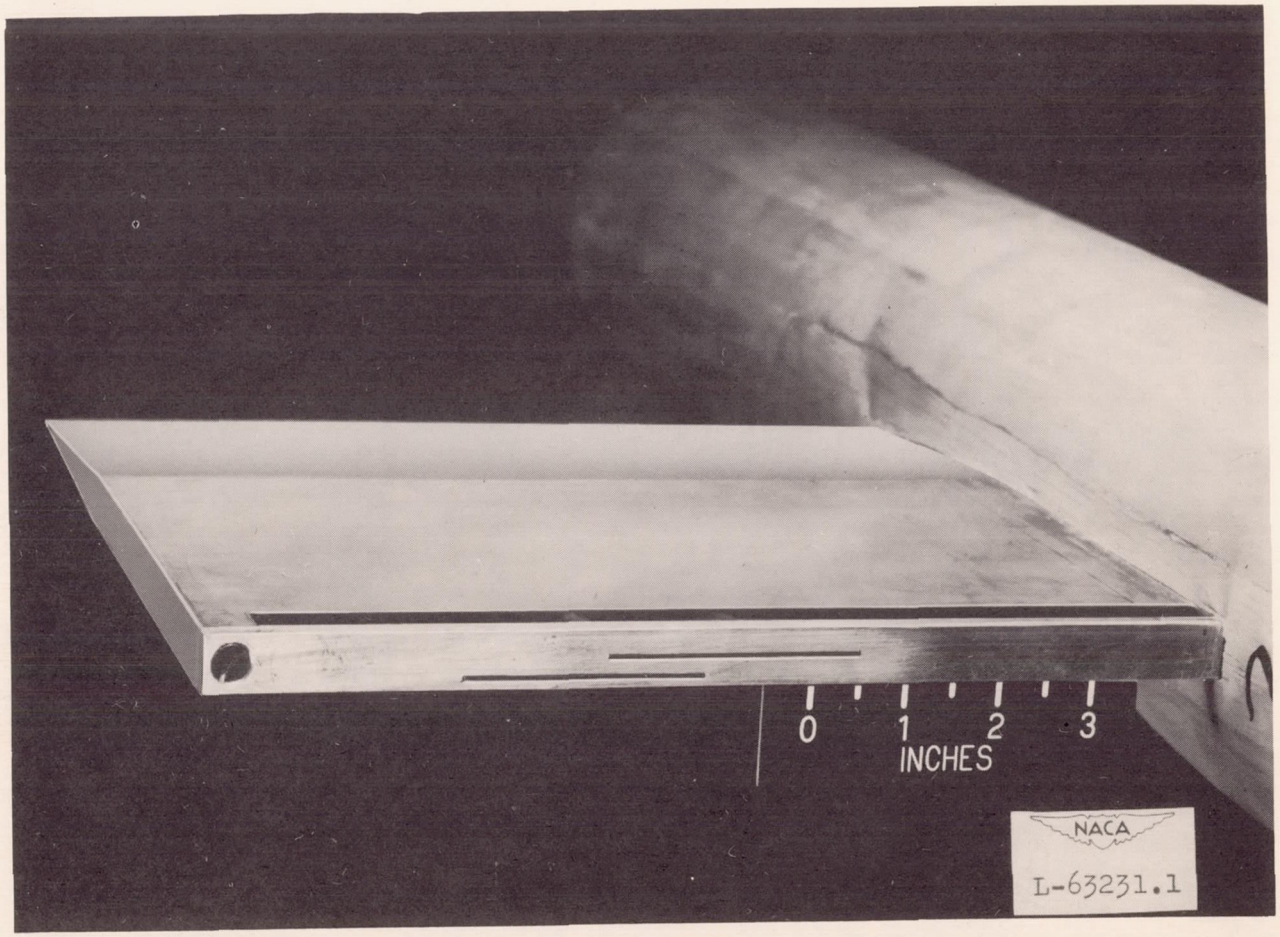

(c) View of pressure slits. (This photograph has been retouched to emphasize pressure slits. The pressure slits are actually 0.02 by 2.5 inches.)

Figure 1.- Concluded.

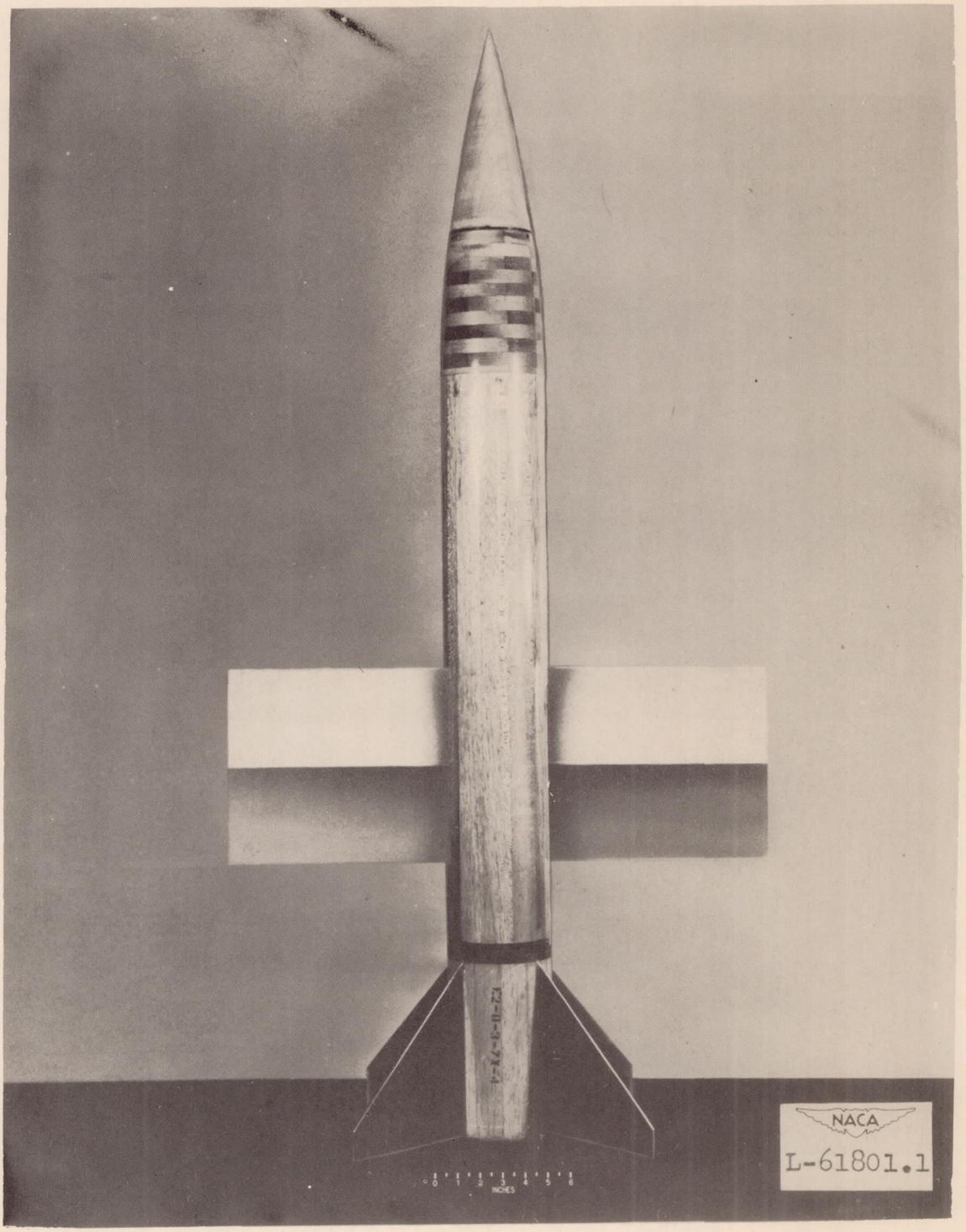

Figure 2.- Photograph showing plan form of diamond-wing-section vehicle.

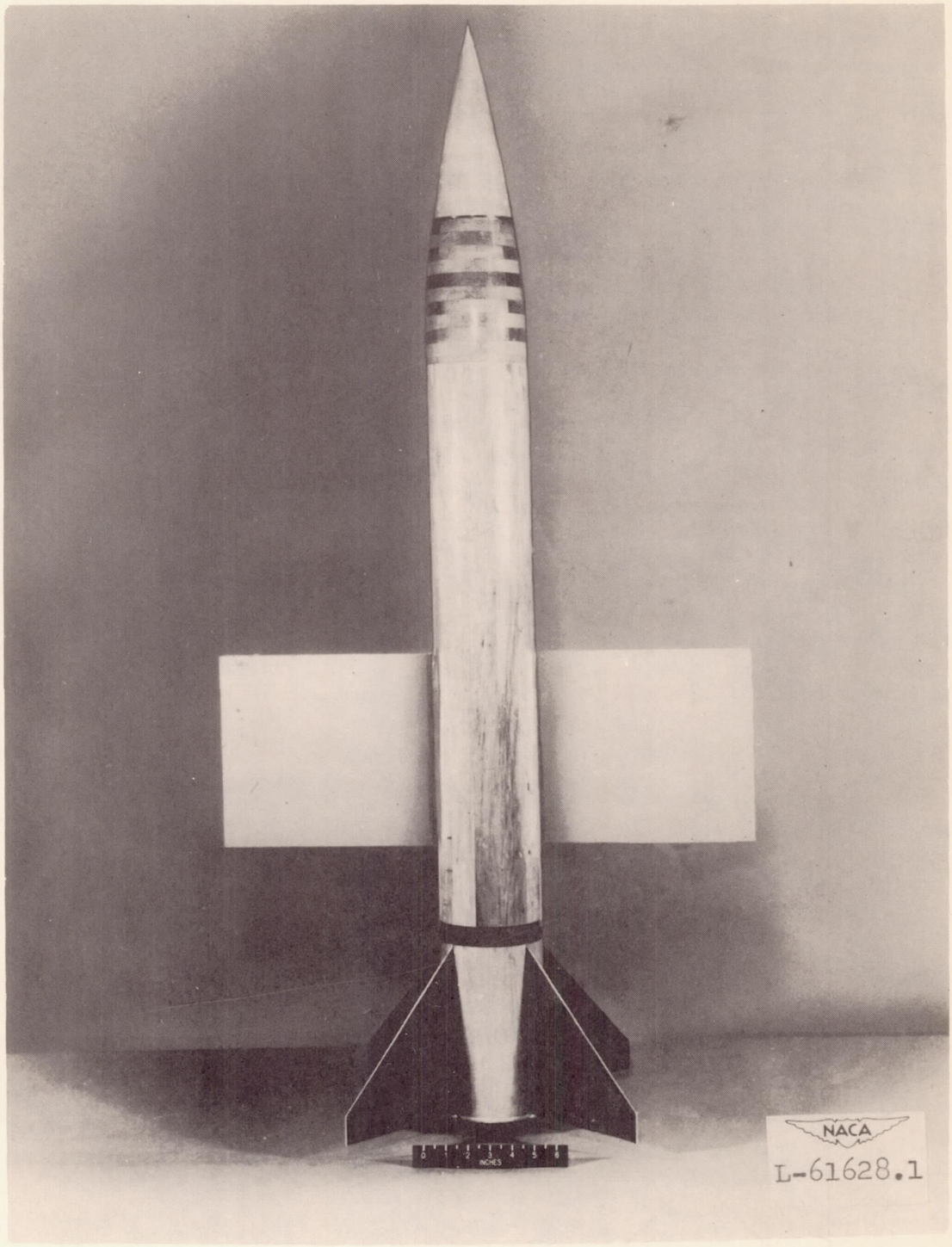

Figure 3.- Photograph showing plan form of circular-arc-wing-section vehicle.

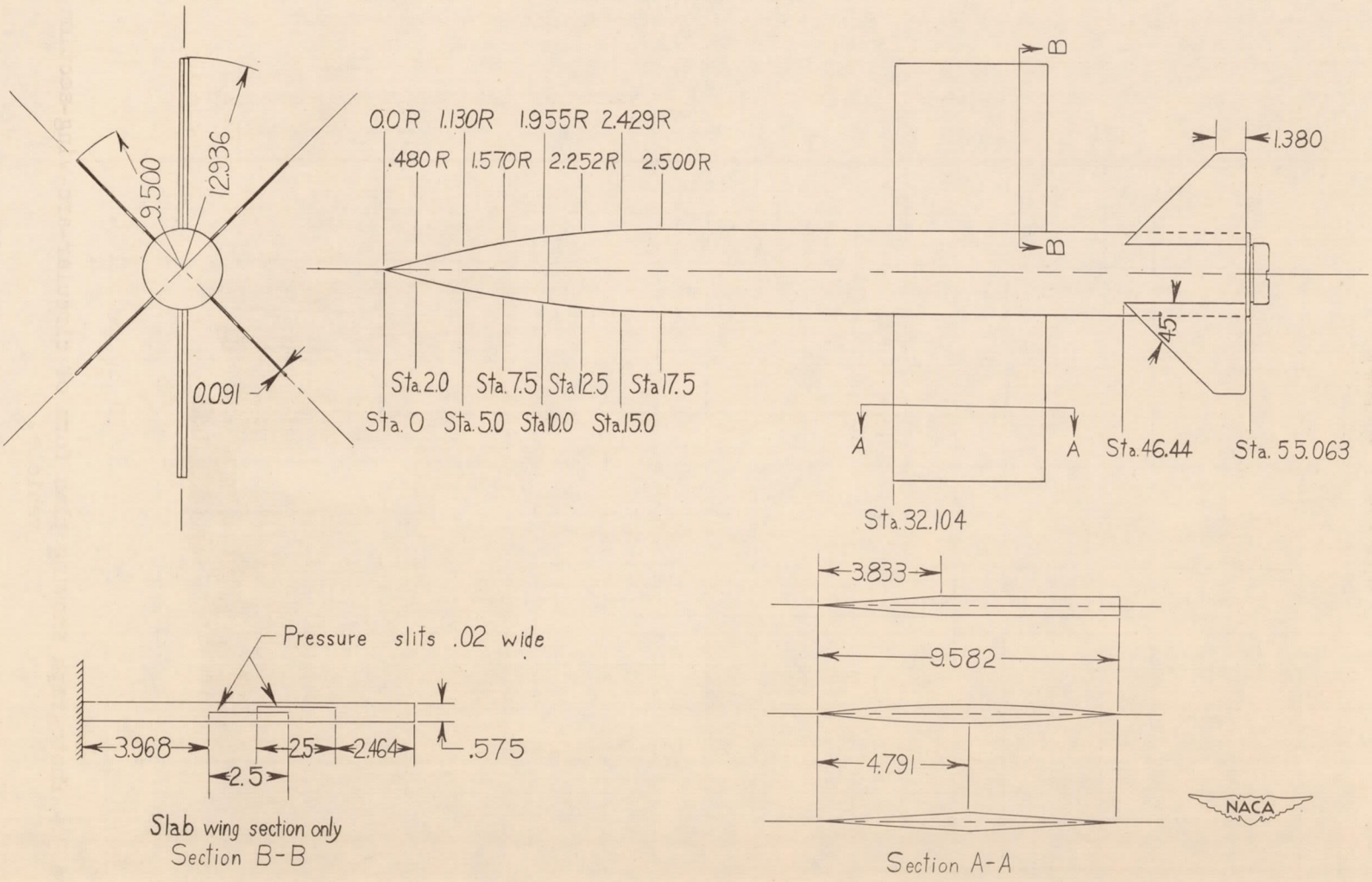

Figure 4.- General arrangement of vehicle showing each section investigated and location of slab base pressure pickups. All sections are 6 percent thick. (All dimensions are in inches.)

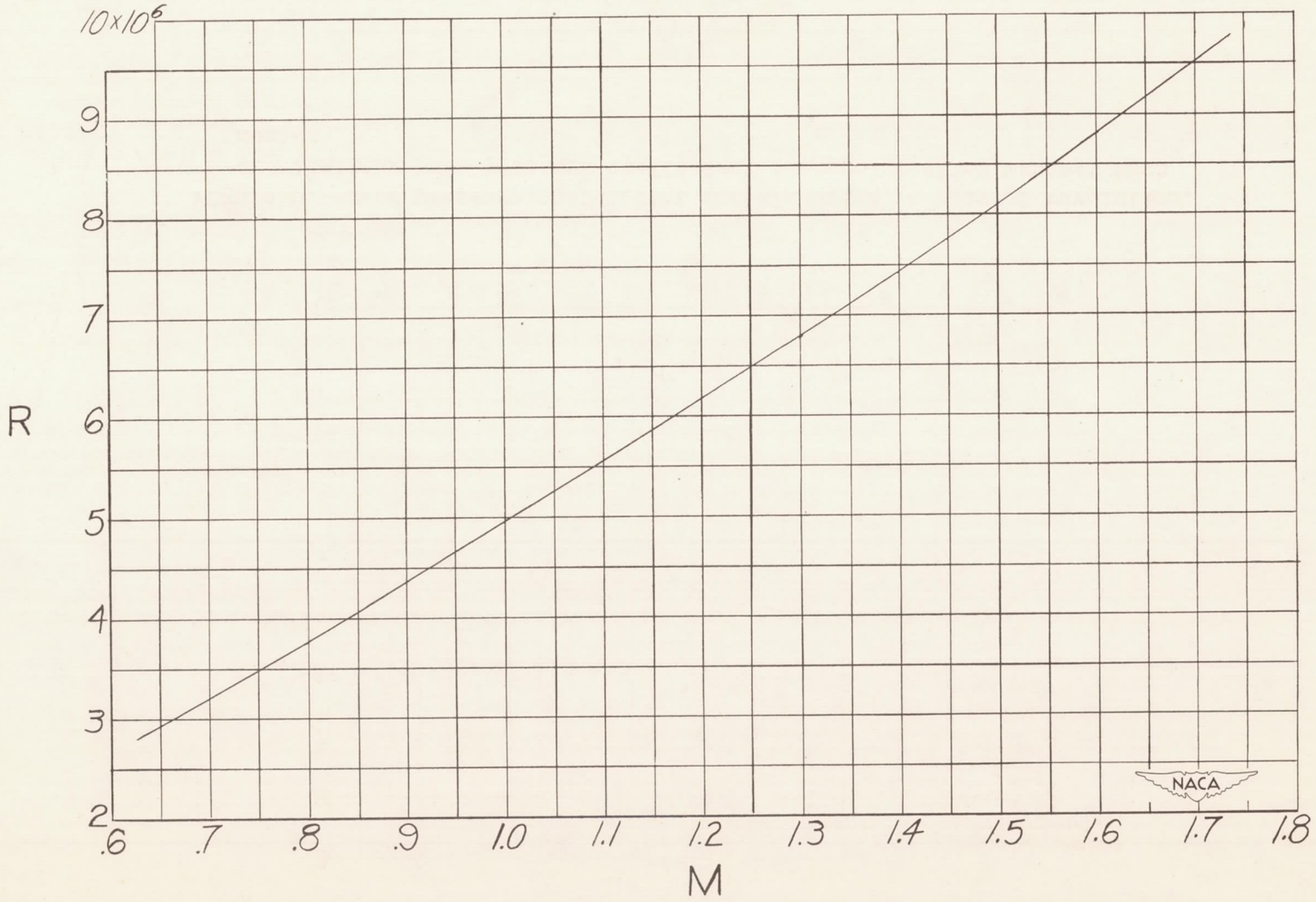

Figure 5.- Reynolds number based on wing chord of 0.798 foot plotted against Mach number.

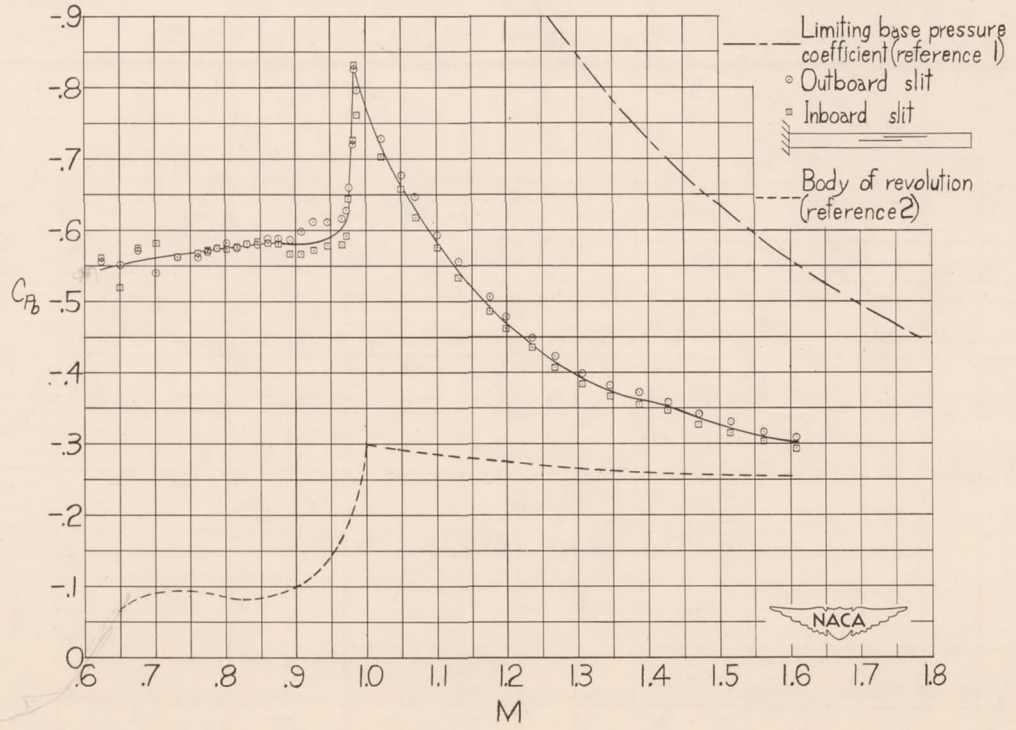

Figure 6.- Base pressure coefficient for slab wing, a body of revolution, and limiting base pressure coefficient (vacuum) plotted against Mach number.

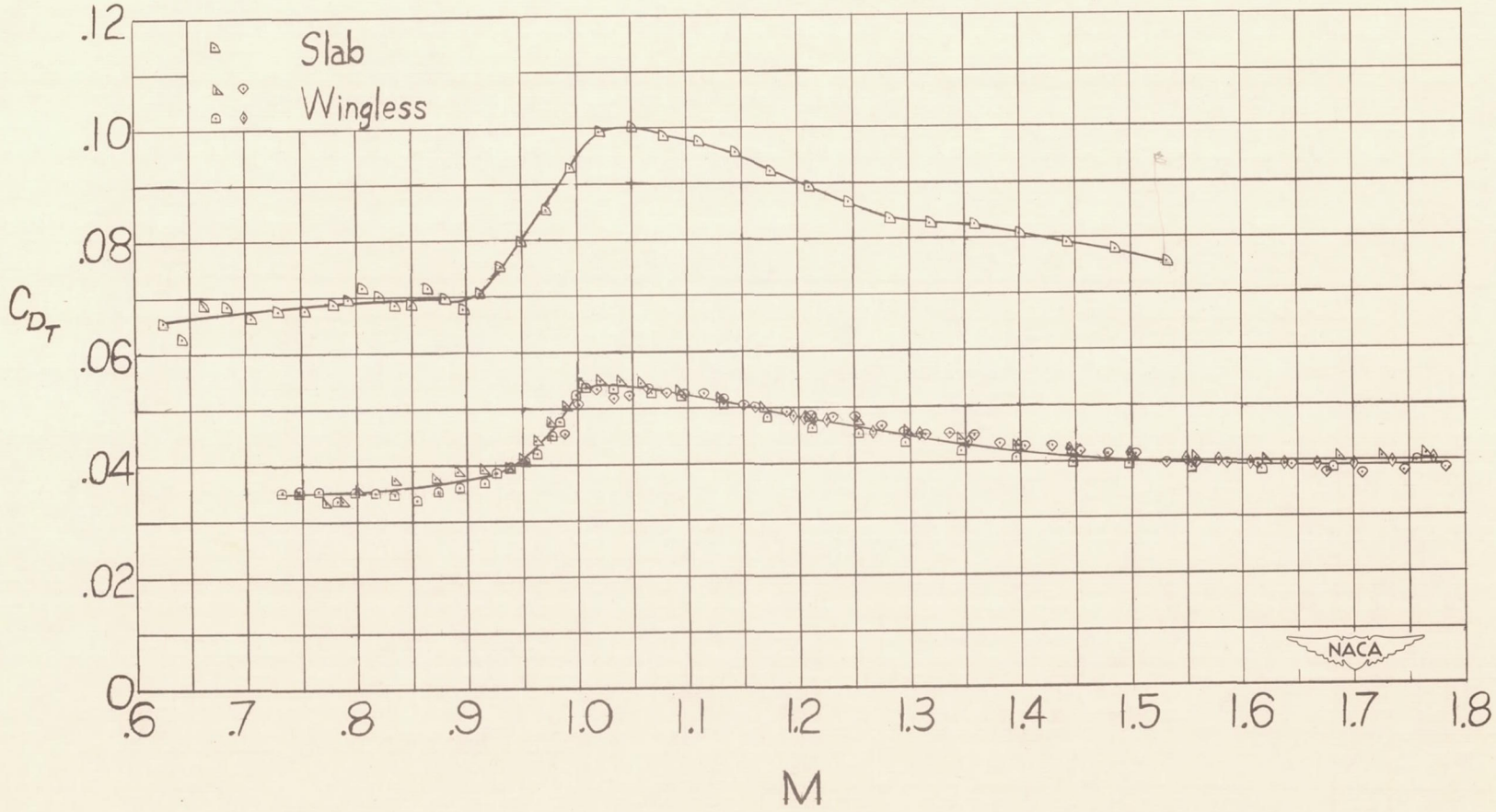

Figure 7.- Total-drag coefficient plotted against Mach number for slab configuration and a wingless configuration. Total-drag coefficient is based on exposed wing area of 200 square inches.

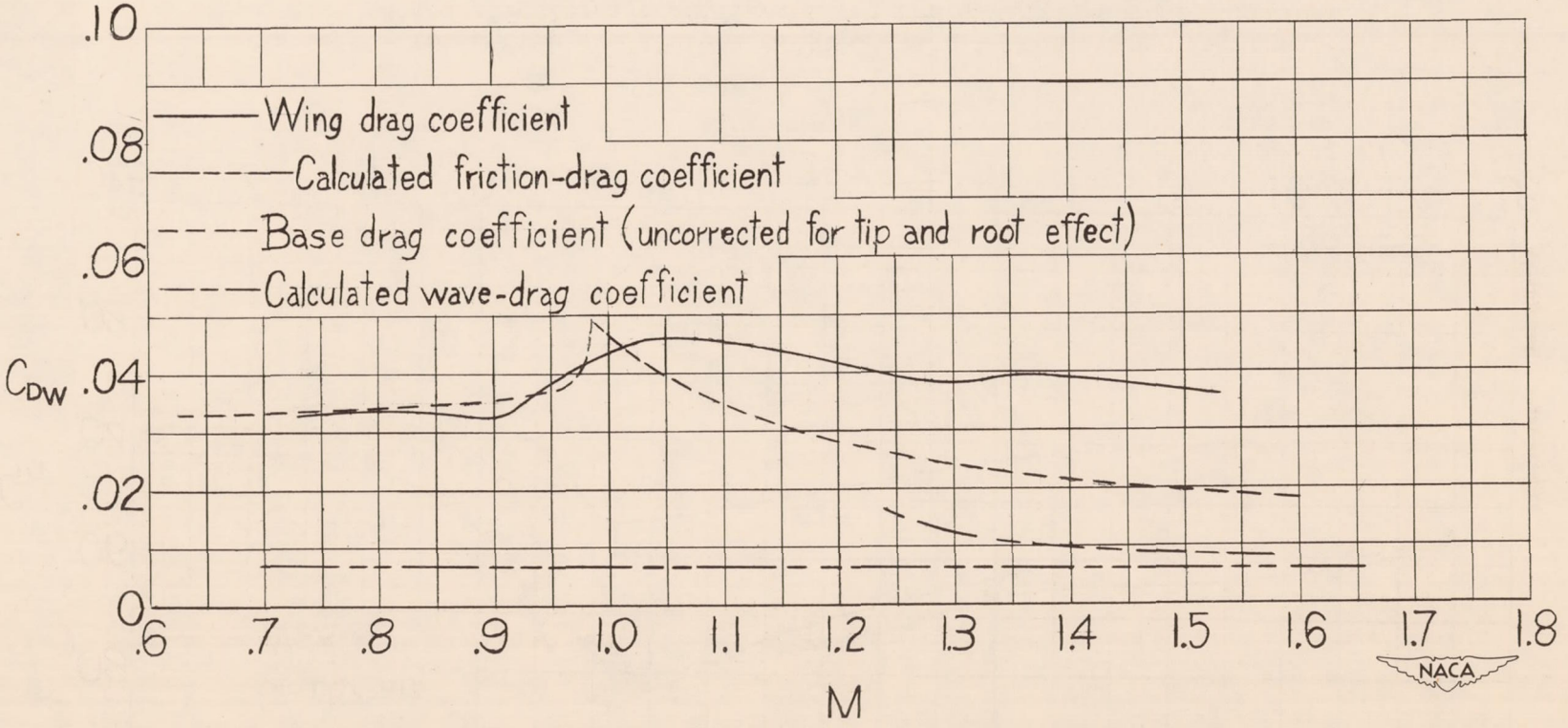

Figure 8.- Comparison of wing, base, and calculated friction- and wave-drag coefficients plotted against Mach number for slab wing.

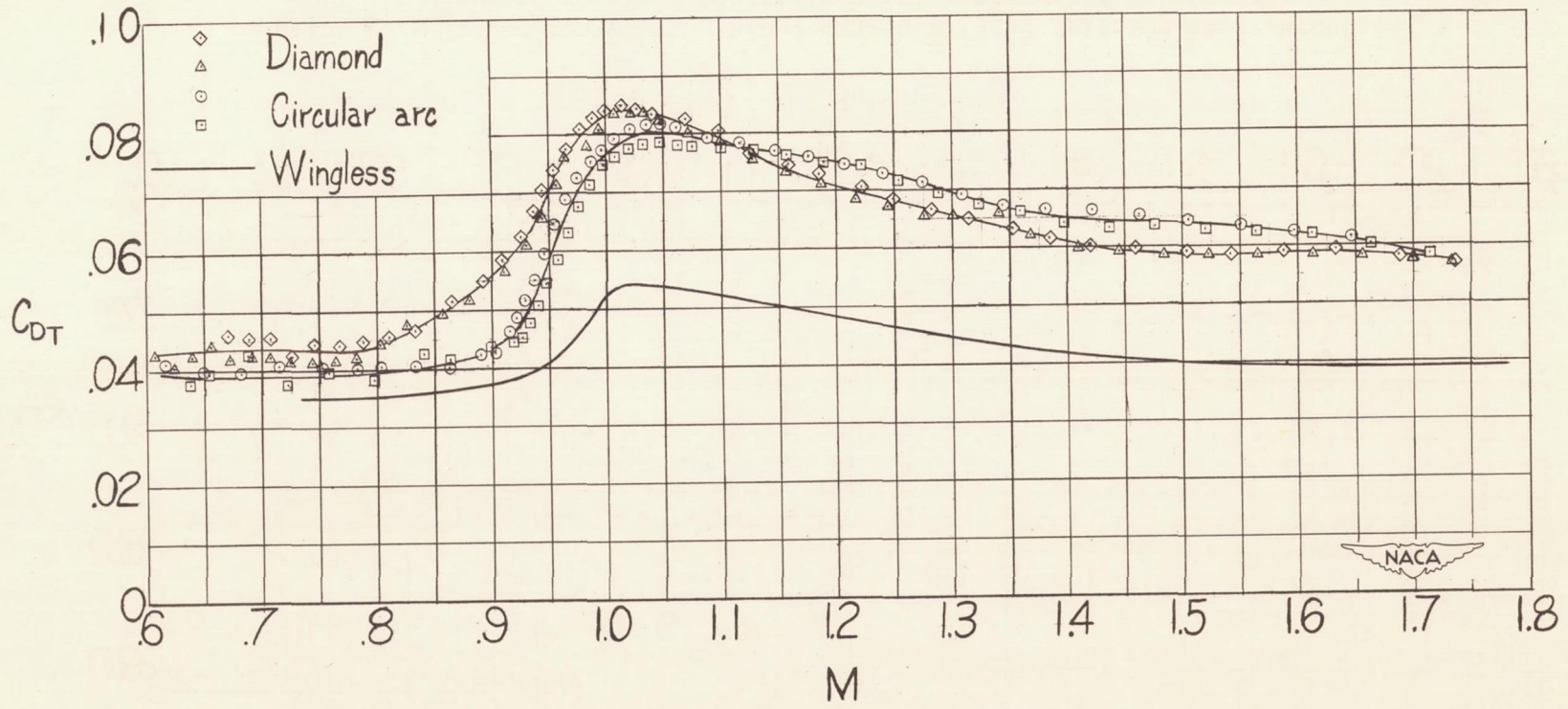

Figure 9.- Total-drag coefficient plotted against Mach number for the diamond and circular-arc configurations and a wingless configuration. Total-drag coefficient is based on exposed wing area of 200 square inches.

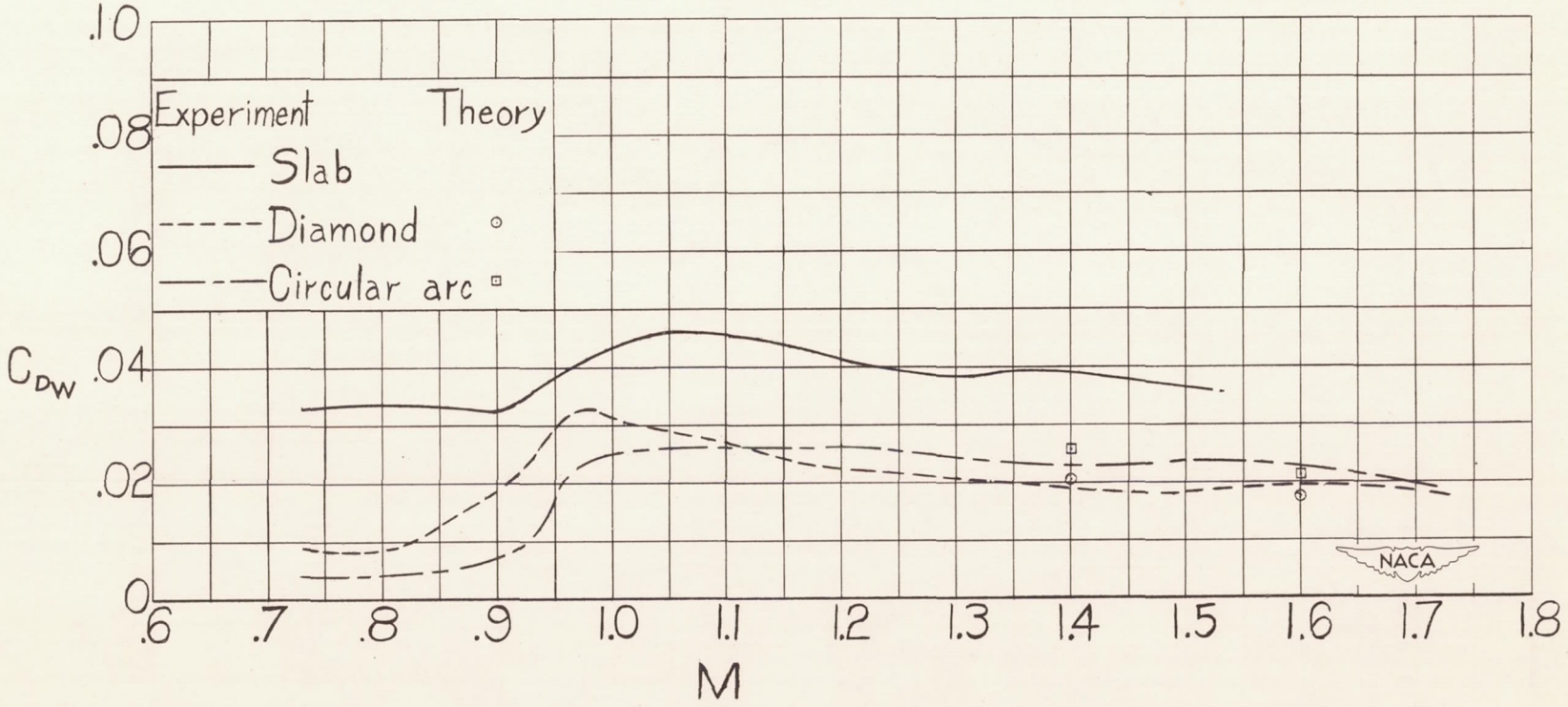

Figure 10.- Comparison of wing-alone drag coefficients for slab, diamond, and circular-arc sections plotted against Mach number. Wing drag coefficients are based on exposed wing area of 200 square inches.